J. Phys.: Condens. Matter 6 (1994) 6557–6564. Printed in the UK

The electronic and magnetic structures of α- and β-manganese

Vladimir Sliwko, Peter Mohn and Karlheinz Schwarz
Technical University of Vienna, Getreidemarkt 9/158, A-1060 Vienna, Austria

Received 21 February 1994, in final form 21 April 1994

Abstract. Band-structure calculations for α- and β-Mn with 58 or 20 atoms, respectively, per unit cell are performed employing the augmented-spherical-wave (ASW) method. For the α-phase a collinear antiferromagnetic spin structure is assumed although some experiments suggest a canting of the spins. The magnetic moments depend on the local environment of the respective atoms and are found to be in good agreement with experiments. β-Mn is found to be a Pauli paramagnet but on the verge of ferrimagnetism. Its electric field gradients as calculated by the ASW method are within the experimental range.

1. Introduction

Manganese exists in four allotropic modifications exhibiting a complex phase diagram [1]. Up to about 1000 K, crystallographically α-Mn is body-centred cubic (BCC) (space group, $I\bar{4}3m$) with 29 atoms per unit cell and four non-equivalent atomic sites (at Wyckoff positions 2a, 8c, and two sets at 24g). Between 1000 and 1370 K, β-Mn is simple cubic (SC) (space group, $P4_132$) with two types of atomic site per unit cell containing 20 atoms (at Wyckoff positions 8c and 12d). For the next 40 K, γ-Mn is face-centred cubic (FCC) and from there up to the melting point at 1517 K the δ-phase has the BCC structure. The magnetic and other physical properties are quite different for the various phases and thus strongly depend on the crystal structure. The explanation of this behaviour is an important problem in the understanding of magnetism in transition metals. The FCC and BCC crystal modification of Mn have already been investigated by various groups using band-structure calculations [2–5]. In the present paper we report band theoretical results for the electronic and magnetic structure of the α- and β-phases whose complicated structures are unique among all elements [6].

The magnetic structure of α-Mn was experimentally determined to be antiferromagnetic with a Néel temperature $T_N = 95$ K [7]. Since the magnitudes of the magnetic moments of the Mn atoms on non-equivalent sites are highly different, antiferromagnetic ordering can only be achieved if the atoms of each Wyckoff position order antiferromagnetically among themselves. Irrespective of several experimental studies it remains unclear whether or not the spins at the different sites are canted with respect to the z axis (for a discussion see Yamada *et al* [8] and references therein). The actual values of the respective magnetic moments, which were deduced from neutron diffraction data, strongly depend on the form factor chosen in the analysis [8]. An NMR study [9] supported these values and derived magnetic moments that are slightly larger than those obtained from the neutron data.

The crystal structure of α-Mn (ignoring magnetism) was illustrated by Daams *et al* [6] who show the nearest-neighbour (NN) configurations of the four non-equivalent sites. The

0953-8984/94/326557+08$19.50

reader is referred to that paper for details and further references. We simplify the magnetic structure by neglecting canting and assume collinear spins. The smallest magnetic unit cell is obtained if we assume antiparallel moments at each pair of the BCC positions (at 0, 0, 0 and $\frac{1}{2}, \frac{1}{2}, \frac{1}{2}$), leading to a simple cubic unit cell with 58 atoms. This choice corresponds to the space group $P\bar{4}3m$. The largest magnetic moments are carried by atoms of types 1 and 2 (Mn(1) and Mn(2)). In figure 1 we show the crystallographic and magnetic structures where we represent opposite spins by dark and light spheres whose radii indicate the magnitude of the respective magnetic moment. Figure 1(*a*) shows the NN shells of Mn(1) which carries the largest magnetic moment. It is surrounded by 12 Mn(4) and 4 Mn(2). The 12 Mn(4) form four equilateral triangles which themselves are tetrahedrally coordinated around the central Mn(1). For each of these triangles the spins are parallel to avoid frustration. The four Mn(2) tetrahedrally surround Mn(1) where, in each tetrahedron, two Mn(2) have + spin and the other Mn(2) have − spin. The second-neighbour shell contains 24 Mn(3) which form eight equilateral triangles centred at the corners of a cube.

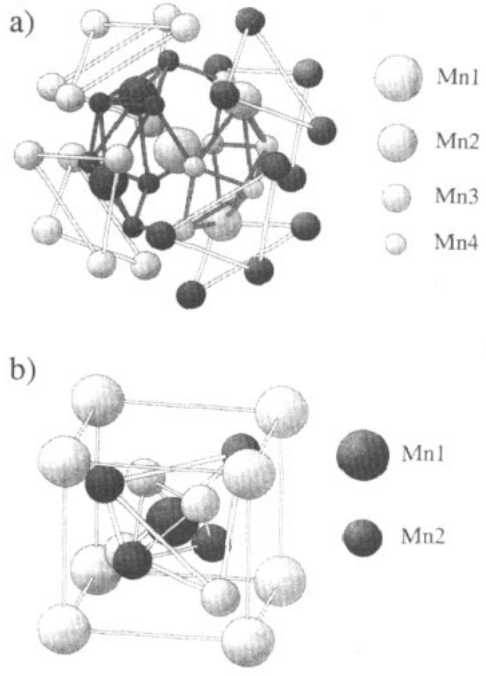

Figure 1. Coordination shell and magnetic structure (dark spheres, spin up; light sphere, spin down) in α-Mn: (*a*) the first-neighbour shells around Mn(1); (*b*) the dominant magnetic structure given by Mn(1) and Mn(2) but omitting Mn(3) and Mn(4) (for details see text).

In figure 1(*b*) we have omitted all atoms with small moments (Mn(3) and Mn(4)) and show the magnetic lattice formed by Mn(1) and Mn(2). The Mn(1) atoms are antiferromagnetically (AF type I) arranged on a BCC lattice and are surrounded by a small tetrahedron and a large tetrahedron of Mn(2), each with two + and two − spins, respectively. For the coordination around Mn(3) and Mn(4) the reader is referred to [6].

The high-temperature phase β-Mn has a SC unit cell with 20 atoms and has been characterized as a Pauli paramagnet with a nearly temperature-independent susceptibility [7].

Antiferromagnetism can be induced by alloying but in pure β-Mn there is no experimental evidence for it. In β-Mn there are two non-equivalent sites that have high coordination numbers (12 and 14, respectively) and a local environment similar to a close-packed structure (comparable with γ-Mn). For a detailed structural analysis we refer the reader to [6].

From these geometrical observations, one should expect the electronic and magnetic structures of both systems under consideration to be understood on the basis of a nearly close-packed environment around each atomic site.

2. The method of calculation

To calculate the electronic and magnetic structures we employ the augmented-spherical-wave (ASW) method [10], an efficient first-principles method for self-consistently calculating the band structure of solids. The calculations are based on the local-spin-density scheme for treating exchange and correlation effects using the parametrization of von Barth and Hedin [11] and Janak [12]. In the ASW method the atomic-sphere approximation (ASA) is used, in which each atom is surrounded by a sphere. Inside each sphere the potential is assumed to be spherically symmetric. The space outside the spheres is neglected but the sum of volumes of all (overlapping) spheres equals the volume of the unit cell. The Brillouin-zone integration is carried out on a grid (in the irreducible wedge) of 20 independent k-points for α-Mn and 45 k-points for β-Mn. The matrix elements are constructed using partial waves up to $l = 2$ (s, p and d states). A contribution associated with the term with $l + 1$ includes corrections due to the internal summation over the three centre integrals. The calculations are carried to self-consistency, which is monitored by the site- and l-projected partial charge, which are well converged to better than 0.0001 electrons. The effect of magnetic order is made possible by allowing spin polarization.

3. Results for α-manganese

In our calculation of the magnetic and electronic structures we use the experimental lattice constant [6] of 16.8075 Bohr and assume a collinear spin arrangement for the magnetic moments at the four different sites as discussed in the introduction. From the magnitudes of the magnetic moments (table 1) we note a clear correspondence to the NN distance. As in FCC (FCT) Mn [4] there exists a critical NN distance for the onset of magnetism, beyond which the magnetic moment increases strongly with increasing NN distance. The largest magnetic moments (and NN distance) is found for Mn(1) and Mn(2), whereas Mn(3) and Mn(4) have relatively small magnetic moments consistent with the small NN distance. Given the simplification of the magnetic structure assumed in the present work and taking into account that our non-relativistic treatment neglects any orbital contributions, there is good agreement in magnitude and mutual orientation (sign) between our calculation and experiment. Our calculation systematically underestimates the magnetic moments but the fact that our collinear spin model agrees fairly well with the experimental interpretation based on canted spins suggests that in α-Mn the canting angle has a minor influence on the absolute value of the magnetic moment, especially for Mn(1) and Mn(2) whose mutual canting angle is small. This result is in agreement with observations that the moments on sites 1 and 2 are more localized rather than itinerant [9], while on sites 3 and 4 a spin-density-wave component was assumed to explain recent hyperfine field measurements [13]. For these latter two sites a significant canting (in various directions) is suggested in the

Table 1. Magnetic moments M of the four non-equivalent sites of α-Mn at the sublattice belonging to (0,0,0). The theoretical values correspond to the experimental lattice constant; the experimental moments are taken from [8,9] and the NN distance from [6].

Site	Number of atoms per unit cell	M (theory) (μ_B/atom)	M(exp) [8] (μ_B/atom)	M(exp) [9] (μ_B/atom)	NN distance [6] (au)
1	2	+1.79	+1.9	+2.05	5.123
2	8	−1.43	−1.7	−1.79	4.707
3	24	−0.40	−0.6	−0.59	4.631
4	24	−0.17	−0.2	−0.28	4.234

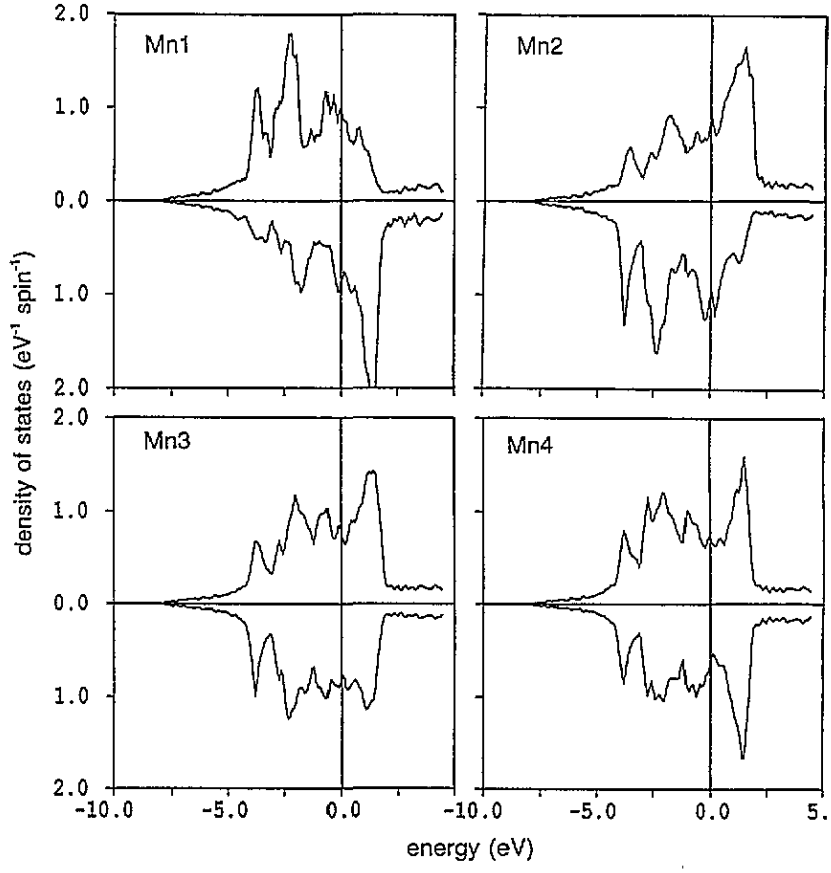

Figure 2. Spin- and site-projected DOS for the four sites in α-Mn.

literature [8,9] so that for these sites a comparison with our collinear-spin results must be taken with caution but the respective moments are small.

In figure 2 we show the spin-projected density of states (DOS) for all four non-equivalent sites which differ significantly and illustrate large deviations from a rigid-band picture. Furthermore they resemble the moments as discussed above, e.g. the large moments for Mn(1) and Mn(2) with opposite sign. The DOS of the latter shows pronounced peaks, indicating a tendency of localization of the magnetic moments corresponding to a flattening of the bands. Given the environment of Mn(1) (figure 1(a)) the Mn(1) DOS can be interpreted

as a 'magnetic impurity state' (for spin down) in a non-magnetic host (Mn(4)), while the small moment on Mn(4) is not genuine but is due to polarization induced by Mn(1). The same situation occurs for Mn(2) in connection with its surrounding Mn(3) and Mn(4). Thus the latter show only small magnetic moments and their DOS resemble that of a close-packed structure.

To calculate the bulk modulus, the variation in the total energy as a function of the lattice constant (volume) was calculated. We observe a strong volume dependence of the individual magnetic moments at the two sublattices similar to the situation that has been found in the antiferromagnetic FCC (FCT) phase [4]. This pronounced magnetovolume coupling in α-Mn leads to a relatively small bulk modulus of 13.9 GPa which—considering the simplifications (neglect of spin canting) in our calculation—is in qualitative agreement with the experimental value of 9 GPa [1]. Both values are much smaller than that of the FCC phase where the bulk modulus of about 30 GPa is found by theory for the non-magnetic case [14]. It is common that the bulk modulus is generally lowered by magnetism especially in antiferromagnets.

The reduction in the bulk modulus due to ferromagnetism is a well known feature for which the following explanation is given: the spin splitting and subsequent transfer of electrons from the minority (spin-down) into the majority (spin-up) bands change the occupation of bonding and antibonding states and thus affect the bonding strength and the equilibrium volume [15].

Although this simple picture explains the magnetovolume effect for ferromagnetic systems, there must be an additional effect in antiferromagnets which usually exhibit an even lower bulk modulus than their ferromagnetic counterpart. Chemical bonding is described by the strength of the overlap between the wavefunctions of neighbouring atoms (if we restrict the interaction to the NN shell). In monatomic ferromagnetic systems (e.g. BCC Fe) the numbers of spin-up and spin-down electrons are the same for any atom in the neighbourhood. In the case of an antiferromagnet (e.g. FCT Mn) the neighbouring atom has exactly the opposite numbers of spin-up and spin-down electrons so that for example wavefunctions of the spin-up electrons of the 'central' atom find only a smaller number of spin-up electrons on the neighbouring site, which reduces the net overlap and thus the bond strength between these atoms. Only the second-nearest neighbour has the same spin as the 'central' atom, but owing to the larger distance the overlap (i.e. the interaction) is reduced. In addition to the changes in occupation numbers (which would be the same for ferromagnets and antiferromagnets), one also observes a systematic change in bonding mechanism which leads to the additional reduction in the bulk modulus in an antiferromagnet.

4. Results for β-manganese

With the equilibrium lattice constant our calculation yields β-Mn as a Pauli paramagnet in agreement with experiment. However, a slight increase in lattice constant leads to the formation of a ferrimagnetic spin alignment where the magnetic moments on the two different types of atoms are antiparallel but differ in magnitude.

The local environment and consequently the corresponding DOS of the two sites in β-Mn are similar to those of Mn(3) and Mn(4) in α-Mn (cf figures 2 and 3). The DOS of β-Mn is shown in figure 3 and resembles that of a close-packed 3d element. The DOS at the Fermi energy is just too small to satisfy the Stoner criterion so that no magnetic instability occurs. Our calculations at the equilibrium volume yield β-Mn to be paramagnetic but with a rather large Stoner enhancement factor of about 7 which suggests that β-Mn is on the verge of

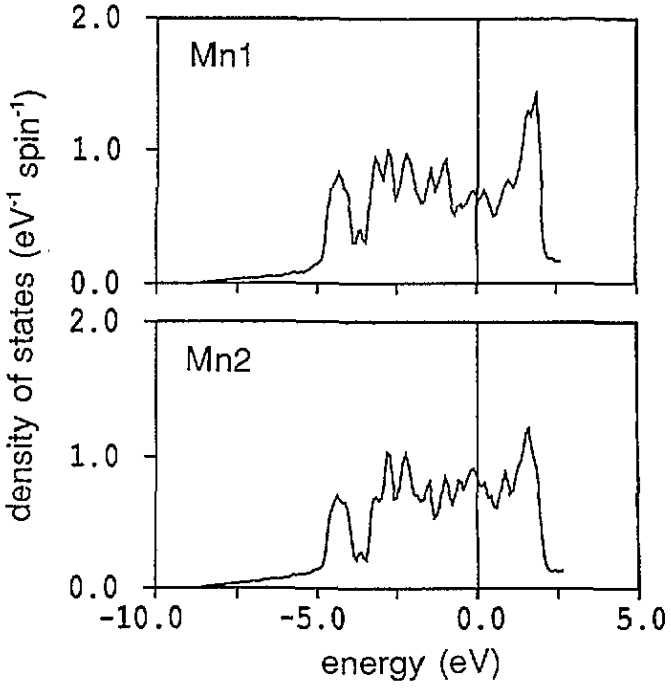

Figure 3. Spin- and site-projected DOS for the two sites in β-Mn.

being magnetic. From the position of the Fermi energy in a minimum of the DOS for atom 1 (figure 3) we can speculate about a possible explanation for the weak temperature dependence of the susceptibility which is found experimentally [7]. If we assume that the finite-temperature properties of this system are governed by collective excitations (spin fluctuations), such a position of the Fermi energy causes a positive coefficient of the linear term in the temperature-dependent susceptibility [16] which would lead to an increase in $\chi(T)$. However, at elevated temperatures any system shows a gradual transition to the *classical* behaviour described by the Curie–Weiss law which is characterized by a $1/T$-dependence of the susceptibility. Since both effects contribute to the total spin susceptibility, their superposition can cause a fairly temperature-independent susceptibility in a certain temperature range.

5. Electric field gradient in β-Mn

Both sites in β-Mn have sufficiently low symmetry to posses a non-vanishing electric field gradient (EFG), which is defined as the second derivative of the electrostatic potential at the nuclear position written as traceless tensor. Recently this EFG has been determined from ^{55}Mn NMR and NQR measurements [17], leading to a nuclear quadrupole coupling constant (NQCC) e^2Qq/h of 1.5–7 MHz ($\eta = 0$) for site I and 30 MHz ($\eta = 0$–0.1) at site II, where e is the electric charge, Q is the nuclear quadrupole moment, q is the principal component of the EFG tensor, h is Planck's constant and η is the corresponding asymmetry parameter. A short review on first-principles calculations of EFGs based on full-potential linearized augmented-plane-wave band-structure results has been given in [18]. In the present work a simplified version of that scheme is used within the ASA following Petrilli and Frota-Pessoa

[19], an approach that should be sufficient for the present systems. Experimentally only the product Qq can be measured but the literature value for Q for ^{55}Mn varies between 0.33 b [20] and 0.55 b [21]. With these values our ASW results of the EFG are converted to a NQCC of 11–18 MHz ($\eta = 0$) for site I and 18–30 MHz ($\eta = 0.4$) for site II. An increase in the lattice constant by 3% (above its equilibrium value) leads to ferrimagnetic ordering (with magnetic moments of $0.15\mu_B$ at site I and $-0.57\mu_B$ at site II) that does not much affect the absolute value of the EFG. However, this increase would reduce the asymmetry parameter at site II to $\eta = 0.08$ which is within the experimental range. For site I the onset of magnetic order does not change the asymmetry parameter η to a finite value.

6. Conclusion

From our band-structure investigation we obtained the electronic and magnetic ground-state properties of α- and β-Mn. The α-Mn phase is found to order antiferromagnetically, where the computed spin magnetic moments are in good agreement with experimental moments. The magnetic moments on Mn(1) and Mn(2) are rather more localized in contrast to those on the sites Mn(3) and Mn(4) which appear to be due only to polarization by the neighbouring local moments. The DOSs of the four different atomic sites are governed by the high coordination numbers and thus are similar to that of the FCC phase for those atoms (Mn(3) and Mn(4)) which carry a low moment. β-Mn is a strongly enhanced Pauli paramagnet and is on the verge of ferrimagnetic order. The position of the Fermi energy in a minimum of the DOS explains the nearly temperature-independent susceptibility which has been observed experimentally. The two different atomic sites in β-Mn have high coordination numbers (similar to the Mn(3) and Mn(4) sites in the α-phase) and thus the DOS is again very similar to the FCC case. The computed EFGs are within the experimental range.

Acknowledgments

This work was supported by the Austrian Science Foundation FWF Projects M025 and M0134. Some of the calculations have been performed on the IBM ES-9000 of the Computer Center at the University of Vienna within the IBM European Academic Supercomputer Initiative.

References

[1] Young D A 1991 *Phase Diagrams of the Elements* (Berkeley, Los Angeles, CA: University of California Press)
[2] Oguchi T and Freeman A J 1984 *J. Magn. Magn. Mater.* **46** L1
[3] Kübler J 1980 *J. Magn. Magn. Mater.* **20** 107
[4] Duschanek H, Mohn P and Schwarz K 1989 *Physica* B **161** 139
Moruzzi V L, Marcus P M and Kübler J 1989 *Phys. Rev.* B **39** 6057
[5] Sliwko V, Blaha P, Mohn P and Schwarz K 1993 *Int. J. Mod. Phys.* B **7** 691
[6] Daams J L C, Villars P and van Vucht J H N 1991 *Atlas of Crystal Structure Types for Intermetallic Phases* vol 4 (Materials Park, OH: American Society for Metals)
[7] *Landolt–Börnstein New Series* 1986 Group III, vol 19 (Berlin: Springer) p 17
[8] Yamada T, Kunitomi N, Nakai Y, Cox D E and Shirane G 1970 *J. Phys. Soc. Japan* **28** 615
[9] Yamagata H and Asayama K 1972 *J. Phys. Soc. Japan* **33** 400
[10] Williams A R, Kübler J and Gelatt C D Jr 1979 *Phys. Rev.* B **19** 6094
[11] von Barth U and Hedin L 1972 *J. Phys. C: Solid State Phys.* **5** 1629

[12] Janak J F 1978 *Solid State Commun.* **25** 53
[13] de Doncker G, Decoster P and Rots M 1992 *Phys. Lett.* **163A** 469
[14] Marcus P and Moruzzi V L 1993 *Phys. Rev.* B **48** 7665
[15] Pettifor D G 1980 *J. Magn. Magn. Mater.* **15–18** 847
[16] Mohn P and Schwarz K 1992 *J. Magn. Magn. Mater.* **104–7** 685
[17] Kohore Y, Noguchi Y and Kohara T 1993 *J. Phys. Soc. Japan* **62** 447
[18] Schwarz K and Blaha P 1992 *Z. Naturf.* a **47** 197
[19] Petrilli H M and Frota-Pessoa S 1990 *J. Phys.: Condens. Matter* **2** 135
[20] Pyykkö P and Li J 1992 *Huki Report* pp 1–92
[21] Javan A 1954 *Phys. Rev.* **96** 649